

Analyzing nitrogen oxides to carbon dioxide emission ratios from space: A case study of Matimba Power Station in South Africa

Janne Hakkilainen^{a,*}, Monika E. Szelag^a, Iolanda Ialongo^a, Christian Retscher^b, Tomohiro Oda^{c,d,e}, David Crisp^f

^a Earth Observation Research, Finnish Meteorological Institute, Helsinki, Finland

^b European Space Agency, ESRIN, Frascati, Italy

^c The Earth from Space Institute, Universities Space Research Association, Columbia, MD, USA

^d Department of Atmospheric and Oceanic Science, University of Maryland, College Park, MD, USA

^e Graduate School of Engineering, Osaka University, Suita, Osaka, Japan

^f Jet Propulsion Laboratory/California Institute of Technology, Pasadena, CA, USA



ARTICLE INFO

Keywords:

Carbon dioxide
Nitrogen oxides
Orbiting Carbon Observatory
TROPOspheric Monitoring Instrument
Emission estimation
Emission ratio
Matimba power station

ABSTRACT

We describe a new methodology for deriving source-specific emission ratios of nitrogen oxides (NO_x) to carbon dioxide (CO_2) from space-based TROPOspheric Monitoring Instrument (TROPOMI) and Orbiting Carbon Observatory-2 (OCO-2) observations. The approach is based on scaling the observed ratio along the OCO-2 track with simulated data, in order to obtain the NO_x -to- CO_2 emission ratio at the source. We analyze fourteen TROPOMI/OCO-2 collocations from near the Matimba coal-fired power station in South Africa. We obtain a mean NO_x -to- CO_2 emission ratio of 2.6×10^{-3} and standard deviation of 0.6×10^{-3} (or 23%). When applied to NO_x emission estimates derived from TROPOMI data, we obtain annual CO_2 emissions of 62, 60 and 58 kt/d for the years 2018, 2019 and 2020, respectively, with standard deviation of 20 kt/d (or 33%). These values are consistent with existing inventories such as the Open-source Data Inventory for Anthropogenic CO_2 (ODIAC). The proposed method will also work ideally for new and upcoming satellite observations systems such as OCO-3, CO2M and GOSAT-GW.

1. Introduction

Anthropogenic emissions from power plants and cities affect both air quality and climate. For example, nitrogen dioxide (NO_2), a precursor to ground-level ozone, is toxic in high concentrations, while carbon dioxide (CO_2) is recognized as the main driver of the observed increase in global temperatures and man-made climate change. These two gases are often co-emitted, but the residence time in the atmosphere for NO_2 (a few hours) is much smaller than for CO_2 (centuries).

The first space-based observations of NO_2 were acquired by the Global Ozone Monitoring Experiment (GOME) between April 1996 and June 2003. These observations were followed by observations made by SCanning Imaging Absorption spectrometer for Atmospheric CHartographY (SCIAMACHY), Ozone Monitoring Instrument (OMI) and GOME-II (Georgoulis et al., 2019). Space-based NO_2 observations have been used in several different applications such as estimating polluting emission rates, analysing long-term changes in the pollution levels and verifying the

success of environmental policy measures (e.g., Beirle et al., 2011; Streets et al., 2013; Krotkov et al., 2016). The TROPOspheric Monitoring Instrument (TROPOMI) was launched on the Copernicus Sentinel 5 Precursor (S5P) in 2017 (Veefkind et al., 2012). TROPOMI provides NO_2 observations with spatial resolution that increased from $3.5 \times 7 \text{ km}^2$ at the beginning of the mission to $3.5 \times 5.5 \text{ km}^2$ since August 6, 2019. This resolution enables the detection of plumes from daily global measurements (Lorente et al., 2019), which was not really possible with its predecessors. For CO_2 observations, SCIAMACHY started taking measurements in 2002 and was followed by Japan's Greenhouse Gases Observing Satellite (GOSAT) in 2009 (Yokota et al., 2009) and NASA's Orbiting Carbon Observatory-2 (OCO-2) in 2014 (Eldering et al., 2017). Recently, the NASA's OCO-3 instrument started providing high-resolution Snapshot Area Maps (SAMs, see also <https://ocov3.jpl.nasa.gov/sams/>) from the International Space Station (Eldering et al., 2019) that are particularly suitable for observing CO_2 emissions from large point sources, such as megacities and power plants (Kiel et al., 2021). The European Commission is currently planning a

* Corresponding author.

E-mail address: janne.hakkilainen@fmi.fi (J. Hakkilainen).

dedicated anthropogenic CO₂ monitoring (CO2M) mission within the Copernicus Programme. In addition, the Global Observing SATellite for Greenhouse gases and Water cycle (GOSAT-GW) mission, including both CO₂ and NO₂ retrievals, is scheduled for launch in 2024.

Beirle et al. (2011) presented one of the first studies for estimating NO_x emissions from point sources using satellite-based observations. Since these first results were presented, several papers using similar techniques have been published (e.g., de Foy et al., 2014; Goldberg et al., 2019). Recently, Beirle et al. (2019) developed a divergence method based on TROPOMI NO₂ data for pinpointing power plant emissions even over a considerably high urban pollution background. On the other hand, satellite-based CO₂ observations have been generally used as input for different inverse modeling systems, but also provided many opportunities to study emissions from megacities and power plants. Nassar et al. (2017) first estimated CO₂ emissions from several power plants applying a Gaussian plume model to OCO-2 satellite data. These cases were re-analyzed by Zheng et al. (2019), who estimated the CO₂ emissions using Weather Research and Forecasting (WRF) model simulations. Reuter et al. (2019) analyzed CO₂ emissions from power plants and cities using collocated TROPOMI and OCO-2 observations and applying the cross-sectional flux method (Varon et al., 2018). The same method was applied to volcanic CO₂ plumes (Johnson et al., 2020). Recently, OCO-2 data together with Lagrangian modeling systems have also been used to infer CO₂ emissions from cities (Wu et al., 2020; Shekhar et al., 2020).

NO₂ emission estimation methods based on satellite observations are often based on statistical analysis, in which the data are averaged over a period of time (one exception is Lorente et al., 2019). On the other hand, satellite-based CO₂ emissions estimation techniques are often based on the use of individual overpasses. Thus, the emission estimation from satellite-observations for NO_x is generally easier than for CO₂ with current measurement systems, because NO₂ is a short lived gas, whose concentrations are increased far above background values, while the CO₂ concentrations in a plume are rarely 1% above the background values. This suggests that it might be advantageous to convert NO_x emissions to CO₂ emissions by using NO_x-to-CO₂ emission ratio. Liu et al. (2020) derived CO₂ emissions using OMI NO₂ observations, but the NO_x-to-CO₂ emission ratios were obtained from inventories and not from observations. The idea of analyzing NO₂ and CO₂ measurements together was also explored earlier by Reuter et al. (2014), who analyzed simultaneous SCIAMACHY NO₂ and CO₂ retrievals in anthropogenic emission areas. Reuter et al. (2019) used TROPOMI NO₂ data to identify the CO₂ plumes and to determine their cross-sectional width. Park et al. (2021) characterized the emission patterns of cities using CO-to-CO₂ and NO₂-to-CO₂ ratios. We have previously studied the OCO-2 column-averaged CO₂ dry air mole fraction (XCO₂) anomalies together with OMI NO₂ using cluster analysis (Hakkarainen et al., 2016) and also calculated CO₂-to-NO₂ ratio over the Highveld emission area in South Africa (Hakkarainen et al., 2019).

In this paper, we want to derive source-specific emission ratios of NO_x to CO₂ directly from space-based TROPOMI and OCO-2 observations. In Sect. 2, we describe the proposed methodology and in Sect. 4.1 we apply it to the TROPOMI/OCO-2 collocated plumes originated from Matimba power station. Finally, we apply the derived NO_x-to-CO₂ emission ratio to the TROPOMI NO_x emissions in Sect. 4.2 and discuss the results in Sect. 5.

2. Methodology

2.1. Cross-sectional flux method

There are several methods for inferring point source emissions from column measurements (Gaussian plume inversion method, source pixel method, integrated mass enhancement method and cross-sectional flux method, see Varon et al., 2018). In the cross-sectional flux method, the emission is obtained by integrating the plume $f(x, y)$ along the y-axis

perpendicular to the wind as

$$C = \int_{-\infty}^{\infty} f(x, y) dy, \quad (1)$$

and then multiplying the integral C with the effective wind speed U_{eff} as

$$E = U_{\text{eff}} \times C. \quad (2)$$

Varon et al. (2018) found a linear relationship with effective wind speed U_{eff} and commonly used 10 m wind speed U_{10}

$$U_{\text{eff}} = \beta U_{10}, \quad (3)$$

with $\beta = 1.3 - 1.5$. We find a similar relationship between 10 m wind and the average wind from different altitudes used here (Sect. 3.2).

For long-lived gases like CO₂ and CH₄, the integral in Eq. (1) is independent of the distance from the source x . In practice with XCO₂ observations given in parts per million by volume, ppm, we obtain $f(x, y)$ from the local anomaly (with respect to the background) as

$$f(x, y) = \frac{XCO_2(\text{anomaly}) \times n_e \times M_{CO_2}}{N_A}, \quad (4)$$

where n_e is the number of dry air particles in the atmospheric column, M_{CO_2} is the molar mass of CO₂ and N_A is the Avogadro's constant. If the shape of $f(x, y)$ is assumed to be Gaussian, the integral can be calculated as

$$C = 0.5 \times \sqrt{\pi/\ln 2} \times a \times \text{FWHM}, \quad (5)$$

where a is the amplitude of the Gaussian function and FWHM is the full width at half maximum. Reuter et al. (2019) applied this method to OCO-2 data, with the FWHM calculated from collocated TROPOMI NO₂ slant-column observations. As the orbit of the OCO-2 instrument is not always perpendicular to the plume, effective normal wind speed was used. In practice, manual adjustment to wind direction is often required, as also pointed out by Nassar et al. (2017).

2.2. Method for the calculation of NO_x-to-CO₂ emission ratios

In principle, the cross-sectional flux can be calculated also using NO₂ observations. However, since the lifetime of NO₂ is short (a few hours), the calculated cross-sectional flux will not be independent of the distance x . Using tropospheric NO₂ columns (given in molecules/cm²), we can express the plume as

$$f_{NO_2}(x, y) = \frac{NO_2(\text{anomaly}) \times M_{NO_2}}{N_A}. \quad (6)$$

If we assume that NO₂ and CO₂ have same cross-sectional form (e.g., Gaussian), and are only separated by different amplitudes, we can calculate the cross-sectional NO_x-to-CO₂ emission ratio at distance x from the source as

$$r(x) = \frac{U_{\text{eff}} \times C_{NO_2}}{U_{\text{eff}} \times C_{CO_2}} = \frac{1.32 \times M_{NO_2}}{n_e \times M_{CO_2}} \times \frac{a_{NO_2}^{\text{obs}}(x)}{a_{CO_2}^{\text{obs}}(x)}, \quad (7)$$

where $a_{CO_2}^{\text{obs}}(x)$ and $a_{NO_2}^{\text{obs}}(x)$ are the amplitudes of the Gaussian function for CO₂ and NO₂, respectively. In order to obtain the cross-sectional NO_x-to-CO₂ emission ratio, we assume a constant value for the NO_x-to-NO₂ ratio of 1.32 with 10% uncertainty, following Beirle et al. (2011).

The cross-sectional ratio depends essentially on the ratio of the amplitudes $r_a(x) = a_{CO_2}^{\text{obs}}(x)/a_{NO_2}^{\text{obs}}(x)$, and it is independent of the wind, except to the extent that NO₂ decays with the distance from the source. The amplitudes can be calculated, for example, by fitting the Gaussian function to the observations, as done by Reuter et al. (2019). The ratio of the amplitudes $r_a(x)$ can be also directly inferred from the data, as shown by Hakkarainen et al. (2019), where the CO₂-to-NO₂ ratio is

determined as the slope of the linear fit between collocated CO₂ and NO_x observations. The advantage of the latter technique is that it can be also applied to more complex non-Gaussian cross-sections.

As the lifetime of NO₂ is short, the cross-sectional NO_x-to-CO₂ emission ratio will differ from the NO_x-to-CO₂ emission ratio at the source. In order to adjust for the effect of the NO₂ decay, we define the correction factor

$$\lambda_{\text{NO}_x}(x) = \frac{E_{\text{NO}_x}^{\text{sim}}}{E_{\text{NO}_x}^{\text{sim}}(x)}, \quad (8)$$

where the denominator $E_{\text{NO}_x}^{\text{sim}}(x)$ indicates the model simulated cross-sectional NO_x flux and the nominator $E_{\text{NO}_x}^{\text{sim}}$ is the emission used in the model simulation. Their ratio should be independent of the actual size of the emission $E_{\text{NO}_x}^{\text{sim}}$. We can also calculate a similar correction factor for CO₂ as

$$\lambda_{\text{CO}_2}(x) = \frac{E_{\text{CO}_2}^{\text{sim}}}{E_{\text{CO}_2}^{\text{sim}}(x)}. \quad (9)$$

In optimal situation, this correction factor should be (close to) one.

The ratio of the correction factors can be calculated as

$$\lambda(x) = \frac{\lambda_{\text{NO}_x}(x)}{\lambda_{\text{CO}_2}(x)} = \frac{E_{\text{NO}_x}^{\text{sim}}}{E_{\text{NO}_x}^{\text{sim}}(x)} \times \frac{E_{\text{CO}_2}^{\text{sim}}(x)}{E_{\text{CO}_2}^{\text{sim}}} = \frac{E_{\text{CO}_2}(x)}{E_{\text{NO}_x}^{\text{sim}}(x)} \times \frac{E_{\text{NO}_x}^{\text{sim}}}{E_{\text{CO}_2}^{\text{sim}}}. \quad (10)$$

Here the first term can be calculated as in Eq. (7):

$$\frac{E_{\text{CO}_2}^{\text{sim}}(x)}{E_{\text{NO}_x}^{\text{sim}}(x)} = \frac{n_e \times M_{\text{CO}_2}}{1.32 \times M_{\text{NO}_2}} \times \frac{a_{\text{CO}_2}^{\text{sim}}(x)}{a_{\text{NO}_2}^{\text{sim}}(x)}, \quad (11)$$

and again the ratio of amplitudes $r_a^{\text{sim}}(x) = a_{\text{CO}_2}^{\text{sim}}(x)/a_{\text{NO}_2}^{\text{sim}}(x)$ can be easily calculated. Now, assuming the units in model simulations and observations are the same, the emission ratio at source can be calculated as

$$r = r(x)\lambda(x) = \frac{a_{\text{NO}_2}^{\text{obs}}(x)}{a_{\text{CO}_2}^{\text{obs}}(x)} \times \frac{a_{\text{CO}_2}^{\text{sim}}(x)}{a_{\text{NO}_2}^{\text{sim}}(x)} \times \frac{E_{\text{NO}_x}^{\text{sim}}}{E_{\text{CO}_2}^{\text{sim}}}. \quad (12)$$

Again, this formula for calculating the emission ratio is independent of the wind and all the terms can be calculated easily and robustly from the observations and model simulations. The correction terms are also quite independent of the actual emissions used, although, we still need to assume that the simulated NO₂ and CO₂ have the same cross-sectional form. One way to look at formula (12) is to interpret it as a correction or an update for the assumed emission ratio $E_{\text{NO}_x}^{\text{sim}}/E_{\text{CO}_2}^{\text{sim}}$, where the correction term is

$$c(x) = \frac{a_{\text{NO}_2}^{\text{obs}}(x)}{a_{\text{CO}_2}^{\text{obs}}(x)} \times \frac{a_{\text{CO}_2}^{\text{sim}}(x)}{a_{\text{NO}_2}^{\text{sim}}(x)} = \frac{r_a^{\text{sim}}(x)}{r_a^{\text{obs}}(x)}. \quad (13)$$

2.3. NO_x emission and lifetime

Beirle et al. (2011) first derived NO_x emissions and lifetimes from space-based NO₂ observations using an exponentially-modified Gaussian model. The method is based on grouping the NO₂ observations according to different wind directions and on calculating NO₂ line densities as the integral perpendicular to the wind direction. The obtained line densities $L(x)$ are fitted by the model function

$$M(x) = Q \times (e^* G)(x) + B, \quad (14)$$

where Q is the emission factor ($E = Q \times U$) given in molecules/m, B is the background (molecules/m), and $(e^* G)(x)$ is the convolution between the Gaussian function G and the exponential decay

$$e(x) = \begin{cases} \exp(-(x - X)/x_0), & x \geq X(\text{downwind}), \\ 0, & x < X(\text{upwind}). \end{cases} \quad (15)$$

Here X is the distance along the wind direction between the linear

density peak and the point source. The NO_x lifetime can be obtained by dividing the e-folding distance x_0 with the wind speed as $\tau = x_0/U$. In practice, five parameters are estimated by fitting: Q , B , X , x_0 , and the width of the Gaussian σ .

Alternatively, before calculating the line densities, the wind rotation technique proposed by Fioletov et al. (2015) can be applied, so that all observations appear to have the same wind direction. This approach has the advantage that all the data can be used together for the fitting, thus reducing the background noise. In this paper, we use the exponentially-modified Gaussian model for estimating monthly NO_x emissions and lifetimes from TROPOMI NO₂ data, after applying the wind rotation around the source, as also shown by Goldberg et al. (2019).

The error estimates related to this method has been discussed extensively in the literature (e.g., Beirle et al., 2011; Fioletov et al., 2015; Goldberg et al., 2019). Assuming that the variables are uncorrelated, we can calculate the total error related to emission estimate using error propagation as

$$\sigma_E = \sqrt{\sigma_{\text{NO}_2}^2 + \sigma_{\text{wind}}^2 + \sigma_{\text{NO}_x/\text{NO}_2}^2 + \sigma_{\text{fit}}^2 + \sigma_{\text{integral}}^2} \quad (16)$$

where all the components are given as relative errors. Following previous research, we assume the uncertainty on the NO₂ tropospheric columns σ_{NO_2} as 30%, the uncertainty related to the wind information σ_{wind} as 20% and the uncertainty on the NO_x-to-NO₂ ratio $\sigma_{\text{NO}_x/\text{NO}_2}$ as 10%. The total error budget is dominated by these components, which yield a total error of 37%. In our analysis, we find that the fitting error σ_{fit} and the error associated with the choice of the integration area σ_{integral} are quite small (both less than 10%). Considering all the error components gives a total error of 40%. In addition, de Foy et al. (2014) found that the lifetimes estimated using this method are close to the chemical lifetimes, although the estimates depend on the accuracy of the plume rotation, and are more likely to be underestimated.

3. Datasets

3.1. Satellite data

We use satellite-based CO₂ observations from NASA's OCO-2 mission and the tropospheric NO₂ product from European TROPOMI instrument.

OCO-2 was launched in 2014 (Crisp et al., 2017) and flies in the A-train on an afternoon polar orbit with equator overpass time around 13:36 local time (LT). OCO-2 measures radiances in the spectral bands near 0.765 μm, 1.61 μm, and 2.06 μm. The retrieval algorithm derives the column-averaged dry air mole fraction of CO₂, XCO₂, using an optimal estimation approach (O'Dell et al., 2018). Each 0.333 s, OCO-2 provides 8 soundings with spatial footprint smaller than 1.29 × 2.25 km² across a narrow swath (less than 10 km wide). In this paper, we use the OCO-2 version V10r lite files, which include bias correction and data screening and are available from NASA's Goddard Earth Sciences Data and Information Services Center (GES DISC, <https://disc.gsfc.nasa.gov>). Previous versions of OCO-2 XCO₂ retrievals have been validated against the Total Carbon Column Observing Network (TCCON) data (Wunch et al., 2017; O'Dell et al., 2018; Kiel et al., 2019). Relative to these earlier versions, the version 10 product used here has both reduced bias and scatter in comparisons to TCCON and other standards (C. W. O'Dell, personal communication). More information about the OCO-2 measurement principle, instrument design, calibration and on-orbit performance can be found in Crisp et al. (2017).

TROPOMI is a passive-sensing hyperspectral nadir-viewing instrument flying onboard the Copernicus Sentinel-5 Precursor satellite since October 2017 (Veefkind et al., 2012). S5P flies on a near-polar sun-synchronous orbit with overpass time of 13:30 LT, similar to OCO-2. TROPOMI measurements in the UV-VIS channel are used in the retrieval of the tropospheric NO₂ columns. The UV-VIS channel spatial resolution at nadir was 7 × 3.5 km² at the beginning of the mission, but

the it has improved to $5.5 \times 3.5 \text{ km}^2$ since August 6, 2019 (van Geffen et al., 2019). We use the TROPOMI NO₂ products versions 1.2 (May 1, 2018–March 20, 2019) and 1.3 (March 20, 2019–November 30, 2020). We only consider data with quality assurance values higher than 0.75 as recommended by the data providers (van Geffen et al., 2019). The TROPOMI NO₂ products are operationally validated by the S5P-MPC-VDAF (S5P – Mission Performance Centre – Validation Data Analysis Facility) using ground-based observations. The operational validation results are periodically reported at the S5P-MPC-VDAF website: <http://mpc-vdaf.tropomi.eu/>. The data are available from Sentinel-5P Pre-Operations Data Hub (<https://s5phub.copernicus.eu/>) and also at NASA's GES DISC.

3.2. Wind data

We use the European Centre for Medium-Range Weather Forecasts (ECMWF) next-generation reanalysis ERA5 dataset (Hoffmann et al., 2019) in the NO_x and CO₂ emission estimation procedures described in Sect. 2. Typically, for the emission estimations based on Gaussian fitting

techniques, winds are averaged over the lowest model altitude layers (e.g. Fioletov et al., 2015, uses the mean from 900, 950 and 1000 hPa layers). However, near the Matimba power station, the mean surface pressure at 12 UTC is only about 910 hPa. For this reason, we use the average winds between 800 and 925 hPa (given at 25 hPa intervals) throughout this study. We use wind fields with $0.1^\circ \times 0.1^\circ$ spatial resolution at 12 UTC. This gives the scaling factor 1.4 between the average wind used here and the 10 m surface wind. This is also the empirical scaling factor found by Varon et al. (2018) and used by Reuter et al. (2019) for the cross-sectional flux method.

3.3. FLEXPART model

FLEXible PARTicle (FLEXPART) is a multi-scale Lagrangian particle dispersion model designed to simulate the transport, diffusion, dry/wet deposition, radioactive decay, and 1st-order chemical reactions of tracers released from different sources (Stohl et al., 2005). The model does not account for chemical reactions between species. Here, we use FLEXPART version 10.4 (Pisso et al., 2019) in forward mode, where concentrations of

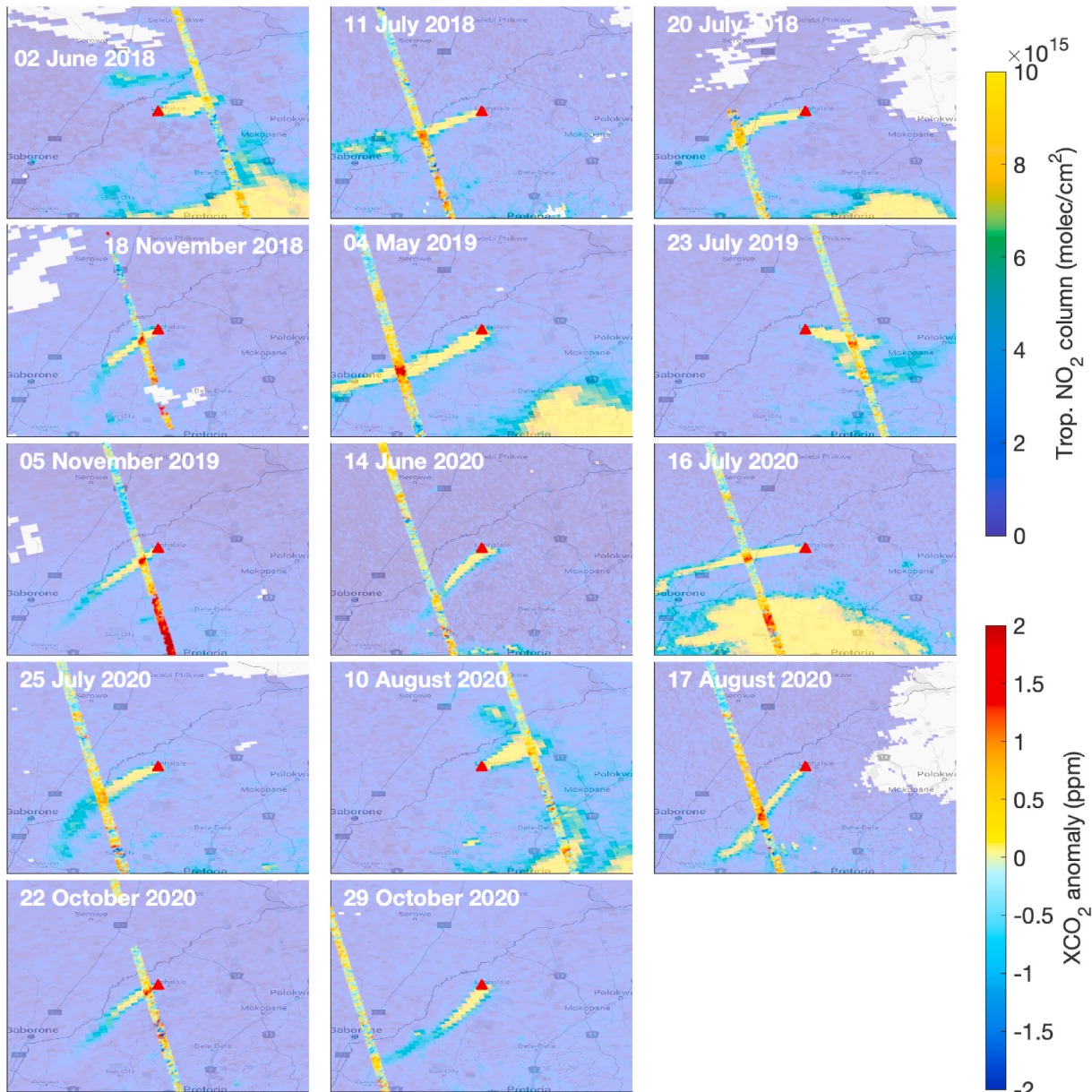


Fig. 1. OCO-2 and TROPOMI observations near Matimba power station (red triangle) in South Africa between May 2018 and November 2020.

the particles released from the source are determined on a regular latitude-longitude grid. FLEXPART is an offline model driven by meteorological fields. For the simulations presented in this study, the ERA5 data from the ECMWF Integrated Forecast System (IFS) were used at $1^\circ \times 1^\circ$ horizontal resolution, with 137 vertical levels and 1 h time resolution. The domain and resolution of the gridded output were $19^\circ\text{--}34^\circ\text{E}$, $19^\circ\text{--}29^\circ\text{S}$ and $0.05^\circ \times 0.05^\circ$, respectively. The number of particles released in each simulations was 100 000 and the release height was 250 m above ground. NO_x simulations were carried out with chemical decay and wet/dry deposition parameters switched on.

4. Results

4.1. Case study of Matimba Power Station in South Africa

Here we apply the methodology described in Sect. 2 to the Matimba coal-fired power station located in South Africa (23.668333°S , 27.610556°E). Matimba is an optimal case study as it is a large isolated emission source with several TROPOMI/OCO-2 collocations. Fig. 1 illustrates 14 collocations found between May 2018 and November 2020. The OCO-2 overpass time is $12:00\text{ UTC} \pm 10$ minutes. The corresponding TROPOMI overpass times are in the range $11:20\text{--}12:29\text{ UTC}$.

For Matimba power station, the Community Emissions Data System (CEDS, Hoesly et al., 2018) reports NO_x emissions of about 172 t/d (or 43 mol/s) for the latest available year 2014, while the Open-source Data Inventory for Anthropogenic CO₂ (ODIAC, Oda et al., 2018) emission dataset (version ODIAC 2020) gives CO₂ emissions of about 70 kt/d for the same time year. Based on these two datasets the NO_x-to-CO₂ emission ratio is about $r = 2.5 \times 10^{-3}$. Tong et al. (2018) reports CO₂ emissions of about 84 kt/d and NO_x emissions of about 260 t/d, which yield the NO_x-to-CO₂ emission ratio of $r = 3.1 \times 10^{-3}$. The Emission Database for Global Atmospheric Research (EDGAR) does not include the emissions from Matimba power station. This was also noted by Reuter et al. (2019), who estimated emissions of 85 ± 19 kt/d by applying the cross-sectional flux method to a single overpass near

Matimba.

We simulate the CO₂ and NO_x concentrations using FLEXPART model for all 14 days presented in Fig. 1. We use an NO_x lifetime of 4 h except for November days when we use lifetime of 2 h. We further discuss the choice of the lifetime value below and in Sect. 4.2. As emission input for Matimba power plant, we use $E_{\text{NO}_x}^{\text{sim}} = 170$ t/d and $E_{\text{CO}_2}^{\text{sim}} = 68.61$ kt/d, giving the ratio $r = 2.48 \times 10^{-3}$. We start the simulations always 36 h earlier than the collocation. Fig. 2 illustrates the CO₂ and NO_x plumes on July 20, 2018 as seen by OCO-2, TROPOMI and FLEXPART. The figure also illustrates the cross-section along the OCO-2 track from both observations and simulated data. The observed and simulated cross-sectional ratios of amplitudes in Eq. (13) are obtained from the slopes of the linear fits between CO₂ and NO_x concentrations as $r_a^{\text{obs}}(x) = 1.06 \times 10^{-16}$ ppm/(molec./cm²) and $r_a^{\text{sim}}(x) = 0.98 \times 10^{-16}$ ppm/(molec./cm²). Using Eq. (12) we obtain the emission ratio:

$$r = \frac{r_a^{\text{sim}}(x)}{r_a^{\text{obs}}(x)} \times \frac{E_{\text{NO}_x}^{\text{sim}}}{E_{\text{CO}_2}^{\text{sim}}} = 2.3 \times 10^{-3}. \quad (17)$$

We have analyzed all the 14 cases shown in Fig. 1 and illustrations like those shown in Fig. 2 are presented for each case in the supplementary material. The results are summarized in Table 1. We calculate the corrected emission ratio using both a linear fit and cross-sectional flux method where possible. For most of the days, the model simulation is quite close to the observations and we are able to carry on all the calculations. The emission ratios obtained with cross-sectional flux method and linear fit are generally similar (see the last two columns in Table 1).

For some days (e.g., May 4, 2019) the model fails to replicate the observed NO_x and CO₂ plumes. We have tested these days using different meteorological datasets (e.g., National Centers for Environmental Prediction, NCEP) and using a different Lagrangian model (Hybrid Single-Particle Lagrangian Integrated Trajectory model, HYSPLIT), but the results remain the same. Overall, we found that FLEXPART simulations with ERA5 produced the closest match to the observed plumes.

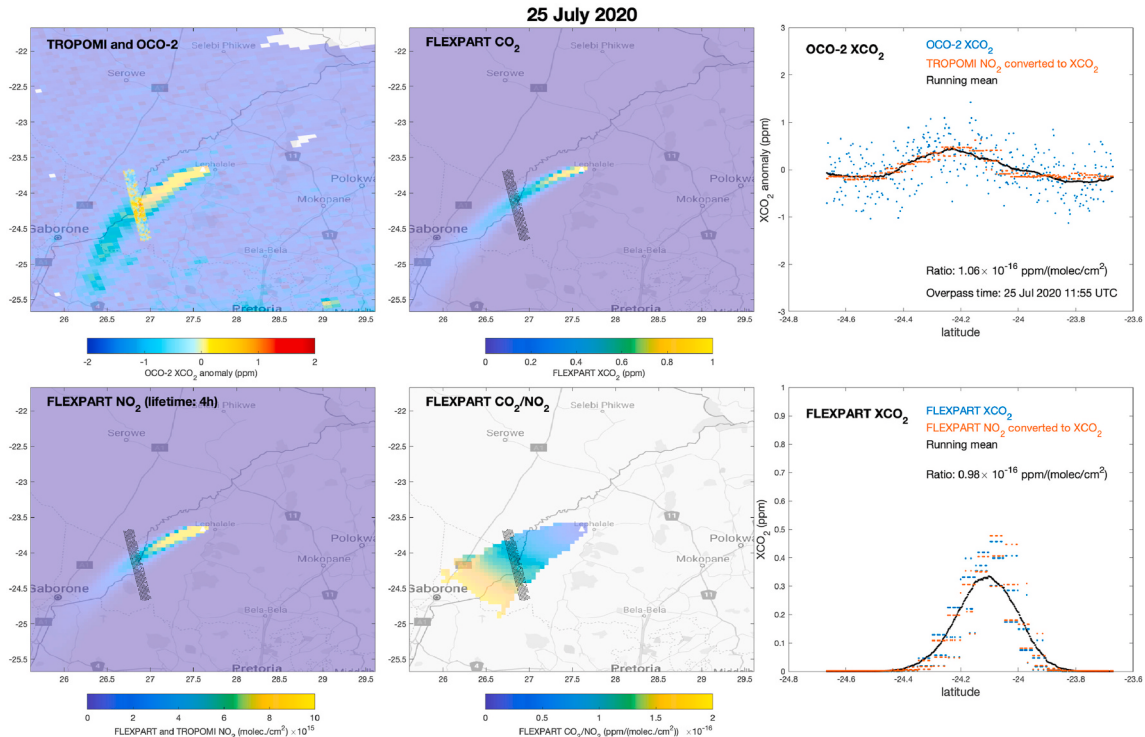


Fig. 2. OCO-2 and TROPOMI observations on July 25, 2020 with FLEXPART model simulations. Similar figures for all 14 cases are shown in the supplementary material.

Table 1
Summary of the satellite overpasses.

Date	Linear fit		Cross-sectional flux (obs.)				Cross-sectional flux (sim.)				Emission ratio ^e	
	$r_a^{\text{obs}}(x)$ ^a	$r_a^{\text{sim}}(x)$ ^a	a_{CO_2} ^b	a_{NO_2} ^c	$r_a^{\text{obs}}(x)$ ^a	E_{CO_2} ^d	a_{CO_2} ^b	a_{NO_2} ^c	$r_a^{\text{sim}}(x)$ ^a	E_{CO_2} ^d	$r(\text{fit})$	$r(\text{flux})$
Jun 2, 2018	0.78	0.92	0.52	0.79	0.65	42	–	–	–	–	2.92	–
Jul 11, 2018	0.98	1.13	1.11	1.06	1.05	61	0.61	0.53	1.15	39	2.87	2.73
Jul 20, 2018	1.01	1.12	0.91	0.87	1.04	70	0.60	0.54	1.12	51	2.75	2.66
Nov 18, 2018	1.02	0.63	1.44	1.30	1.11	107	0.41	0.67	0.61	66	1.52	1.37
May 4, 2019	0.93	–	1.90	1.88	1.01	126	–	–	–	–	–	–
Jul 23, 2019	0.69	0.64	1.01	0.99	173	0.46	0.81	0.56	53	2.29	1.40	
Nov 5, 2019	1.15	0.51	1.55	1.06	1.46	146	0.53	1.03	0.51	47	1.10	0.87
Jun 14, 2020	1.06	1.62	0.64	0.48	1.34	7	0.25	0.15	1.6	13	3.78	2.95
Jul 16, 2020	0.83	0.63	1.44	1.60	0.90	159	0.36	0.58	0.63	45	1.87	1.73
Jul 25, 2020	1.06	0.98	0.68	0.59	1.15	47	0.41	0.41	0.99	29	2.30	2.13
Aug 10, 2020	0.54	1.42	0.50	0.91	0.55	21	0.54	0.35	1.54	31	6.54	7.01
Aug 17, 2020	1.43	1.20	1.29	0.71	1.83	104	–	–	–	–	2.09	–
Oct 22, 2020	1.33	0.35	1.41	0.95	1.48	83	0.68	1.95	0.35	40	0.64	0.58
Oct 29, 2020	1.97	1.83	0.73	0.17	4.24	68	0.18	0.10	1.83	37	2.30	1.07

^a value $\times 10^{-16}$ ppm/(molec./cm²).

^b ppm.

^c value $\times 10^{16}$ molec./cm.²

^d CO₂ emission (kt/d) calculated using the cross-sectional flux method as in Reuter et al. (2019), using both OCO-2 observations (obs.) and FLEXPART simulation (sim.).

^e Emission ratio (value $\times 10^{-3}$) calculated using linear fit and cross-sectional flux method as in Eq. (17).

For three days (November 18, 2018, November 5, 2019 and October 22, 2020) we observe the OCO-2 overpass very close to the emission source (about 25 km). In fact, these three days are part of the same 16-day repeat cycle. During these days, the ratio of amplitudes from the simulations is relatively low, even if we use shorter prescribed NO₂ lifetime (i.e., 2 h). This yields also lower emission ratios. Part of the reason could be that NO₂ has not yet been substantially oxidised and lower NO₂ values yields higher ratios of amplitudes near the emission source. Further reducing the prescribed NO₂ lifetime, would cause the model to fail in replicating the observed NO₂ plume.

In order to calculate the mean NO_x-to-CO₂ emission ratio, we select nine of the fourteen calculated emission ratios (bolded values in Table 1). We exclude the values of the three days with collocation very close to the source, and also the value obtained on August 10, 2020. The resulting mean value is 2.6×10^{-3} , with standard deviation of 0.6×10^{-3} .

To further study the effect of NO₂ lifetime, we repeat the analysis assuming lifetimes of 2, 3, 4, 5 and 6 h in the FLEXPART simulations. The results are summarized for nine selected days in Fig. 3. As expected, the NO_x-to-CO₂ emission ratio decreases with increasing lifetime following an exponential decay. For example, assuming the lifetime of 3 h and 5 h in the model simulations yields mean ratios of $(4.0 \pm 1.2) \times 10^{-3}$ and $(2.0 \pm 0.4) \times 10^{-3}$, respectively. Fig. 3 illustrates that assuming too low lifetime yields unrealistic results while increasing the lifetime values affects the emission ratio gradually less.

For comparison, we also calculate the CO₂ emissions using the cross-sectional flux method as described by Reuter et al. (2019). For this purpose, we use the wind speed and direction from the ERA5 data set as described in Sect. 3.2 and manually correct the wind direction. This choice is slightly subjective, and thus we report the best estimate only (Table 1). We observe quite large variation in the resulting CO₂ emission estimations, with a mean value 87 kt/d and standard deviation 51 kt/d. For example, we obtain emissions of 7 kt/d, 159 kt/d and 47 kt/d during June and July 2020, although this variability is only partly due to the correction of the wind direction. For completeness, we applied the cross-sectional flux method to the simulated data as well, and treated the simulations as they would have been satellite observations (Table 1). In this case, we obtain CO₂ emissions between 13 kt/d and 66 kt/d that are always lower than the values used as input in the simulations ($E_{\text{CO}_2}^{\text{sim}} = 68.61$ kt/d). In cases like on June 14, 2020, this indicates that the cross-sectional flux is not always a good estimate of the CO₂ emission, as the observations also give a very low value of the cross-sectional emissions (7 kt/d). The results might also indicate that the effective wind

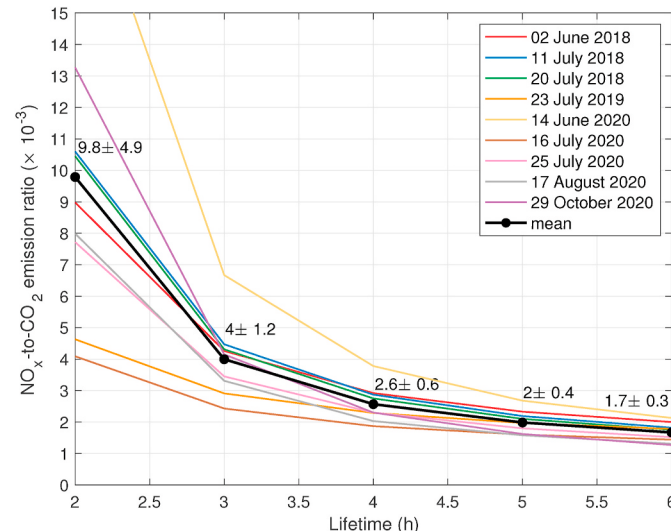


Fig. 3. NO_x-to-CO₂ emission ratios assuming different lifetimes in the FLEXPART simulations.

speed needs to be corrected (see Eq. (2)). On the other hand, in some cases the cross-sectional emissions derived from the observations are about a factor of 2 higher than the expected value of about 70 kt/d.

4.2. NO_x emission estimation and application of the NO_x-to-CO₂ emission ratio

In order to calculate the NO_x emissions from Matimba power station, we apply the wind rotation technique to the TROPOMI NO₂ tropospheric columns as described by Fioletov et al. (2015) and Goldberg et al. (2019). We select only TROPOMI data corresponding to wind speed between 2 and 6 m/s and then calculate the monthly and annual means. Fig. 4 illustrates the NO₂ distribution around the source after the rotation for each month and for the whole year 2019. The data are oversampled to $0.01^\circ \times 0.01^\circ$ resolution and the local background (median) is removed. The NO₂ distribution appears now as the wind direction for all observations is out of the west. For each panel shown in Fig. 4, we calculate the line density as the integral over the across-wind direction

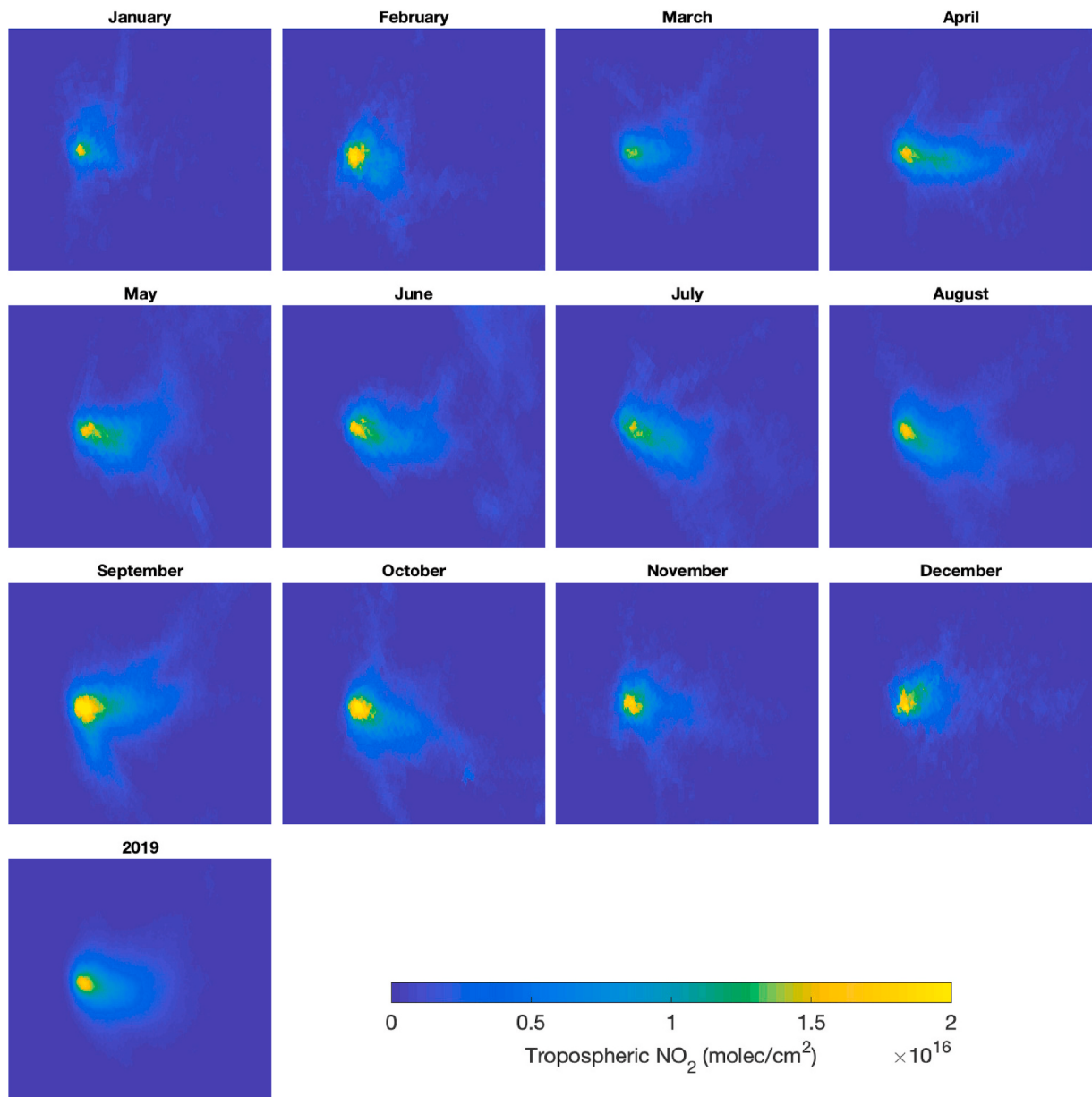


Fig. 4. Wind-rotated TROPOMI monthly and annual NO₂ means for the year 2019. The data are oversampled to $0.01^\circ \times 0.01^\circ$ resolution and the local background (median) is removed.

(Fig. 5). In order to estimate NO_x lifetime and emission, we use the method described in Sect. 2.2 and fit the line densities with the exponentially-modified Gaussian function described in Eq. (14). The resulting NO_x emissions and lifetimes are presented in Fig. 6 (red circles in the upper and middle panels, respectively). We observe seasonality in both emissions and lifetime, with the variables somewhat anti-correlated. On average, the NO_x lifetime is around 4 h (horizontal red lines in Fig. 6, middle panel), which is the value we use for most days in the Lagrangian model simulations. Beirle et al. (2019) also used a constant lifetime of 4 h over South African Highveld area throughout the year and assumed that seasonal dependencies can be neglected. Nevertheless, our estimated lifetimes are somewhat smaller between November and February, and we use therefore a lifetime of 2 h when calculating the ratios for the November overpasses. In general, shorter lifetimes are expected during (austral) summertime due to accelerated photochemistry (e.g., Goldberg et al., 2020).

The annual emissions are 44, 43 and 41 mol/s for 2018, 2019 and 2020, respectively (horizontal red lines in Fig. 6, upper panel). The

standard deviation of the monthly means is 11 mol/s, which is about 25–30% of the annual values. As discussed in Sect. 2.2, the total error associated with the individual NO_x emission estimates is about 40%, although the fitting error and the error due to the section of the integration area are less than 10%.

Overall, the NO_x emissions derived from TROPOMI data are quite close to the values reported in the CEDS database (43 mol/s for 2014), even if the latter monthly values do not change sensibly during the year. The grey crosses in Fig. 6 indicate the monthly NO_x emissions tabulated from the Eskom's emission reports (available online at <https://www.eskom.co.za/Whatweredoing/AirQuality/Pages/Matimba-Power-Station.aspx>). The TROPOMI-based annual NO_x emissions are slightly smaller than the annual value reported by the company (55 mol/s), but the difference remains within the errors.

Finally, we apply the mean emission ratio r derived in Sect. 4.1 to the TROPOMI-estimated NO_x emissions $E_{\text{NO}_x}^{\text{est}}$ to derive the CO₂ emission estimates as

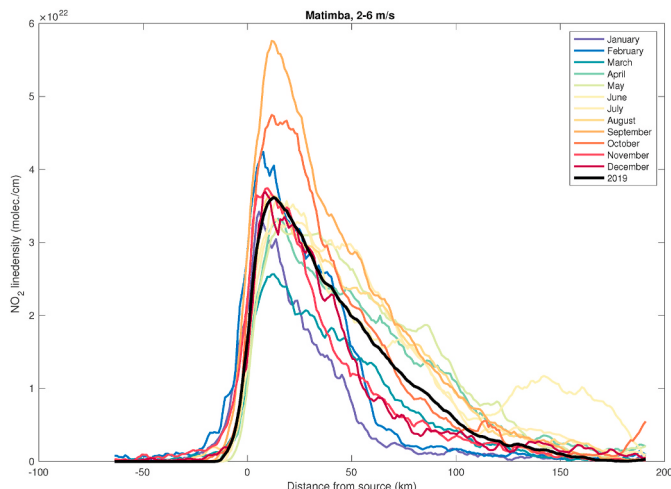


Fig. 5. TROPOMI monthly and annual NO_2 mean line densities for the year 2019. The line densities are calculated from the data illustrated Fig. 4.

$$E_{\text{CO}_2}^{\text{est}} = \frac{E_{\text{NO}_x}^{\text{est}}}{r}. \quad (18)$$

Assuming that the errors in $E_{\text{NO}_x}^{\text{est}}$ and r are uncorrelated and using the standard propagation of errors we have that

$$\sigma_{E_{\text{CO}_2}^{\text{est}}}^2 \approx \left(E_{\text{CO}_2}^{\text{est}} \right)^2 \left(\left(\frac{\sigma_{E_{\text{NO}_x}^{\text{est}}}^{\text{est}}}{E_{\text{NO}_x}^{\text{est}}} \right)^2 + \left(\frac{\sigma_r}{r} \right)^2 \right). \quad (19)$$

As error estimates, we consider the sample standard deviations $\sigma_{E_{\text{NO}_x}^{\text{est}}}^{\text{est}} = 11 \text{ mol/s}$ and $\sigma_r = 0.6 \times 10^{-3}$. These error estimates may be too large for typical random errors, but in this case the errors are likely to be systematic with possible seasonal component, rather than random. For

example, TROPOMI NO_2 tropospheric columns are expected to have a negative bias over polluted areas due to inaccurate a priori information used in the retrieval. However, this systematic error should cancel out in Eq. (18), where the same bias would be in both numerator and denominator. In addition, there can be systematic errors in r due to the choice of the lifetime assumed in the model simulations.

The blue error bars in Fig. 6 (bottom panel) indicate the uncertainties in CO_2 emissions when only the errors in the emission ratio are considered, while the red error bars indicate the total error. In addition, Fig. 6 (bottom panel) includes the monthly ODIAC CO_2 emissions for the year 2018 and 2019 (green crosses) and the CO_2 emissions obtained using the cross-sectional flux method (black crosses), reported also in Table 1. The CO_2 annual emission values are 62, 60 and 58 kt/d for the years 2018, 2019 and 2020, respectively, with uncertainty of 20 kt/d (or 33%) derived according to Eq. (18).

We find that the CO_2 emissions agree within the errors with the ODIAC monthly estimations. On the other hand, the agreement with the estimates based on the cross-sectional flux is quite variable, due to the large variability of the estimates based on daily collocations.

5. Summary and discussion

In this paper, we developed a new methodology to derive NO_x -to- CO_2 emission ratios from space-based OCO-2 and TROPOMI observations. The approach is based on the analysis of the collocated OCO-2 CO_2 and TROPOMI NO_2 concentrations along the OCO-2 track. In order to scale the cross-sectional emission ratio to the emission ratio at the source, we derive a correction factor based on model simulations. We applied the methodology to 13 of the 14 collocations found over the Matimba power plant and we derived the mean NO_x -to- CO_2 emission ratio with its standard deviation as $(2.6 \pm 0.6) \times 10^{-3}$.

Our approach is derived from the cross-sectional flux formulation, but the calculation of the ratio does not need a Gaussian shape assumption, as it can be directly obtained from the linear fit between

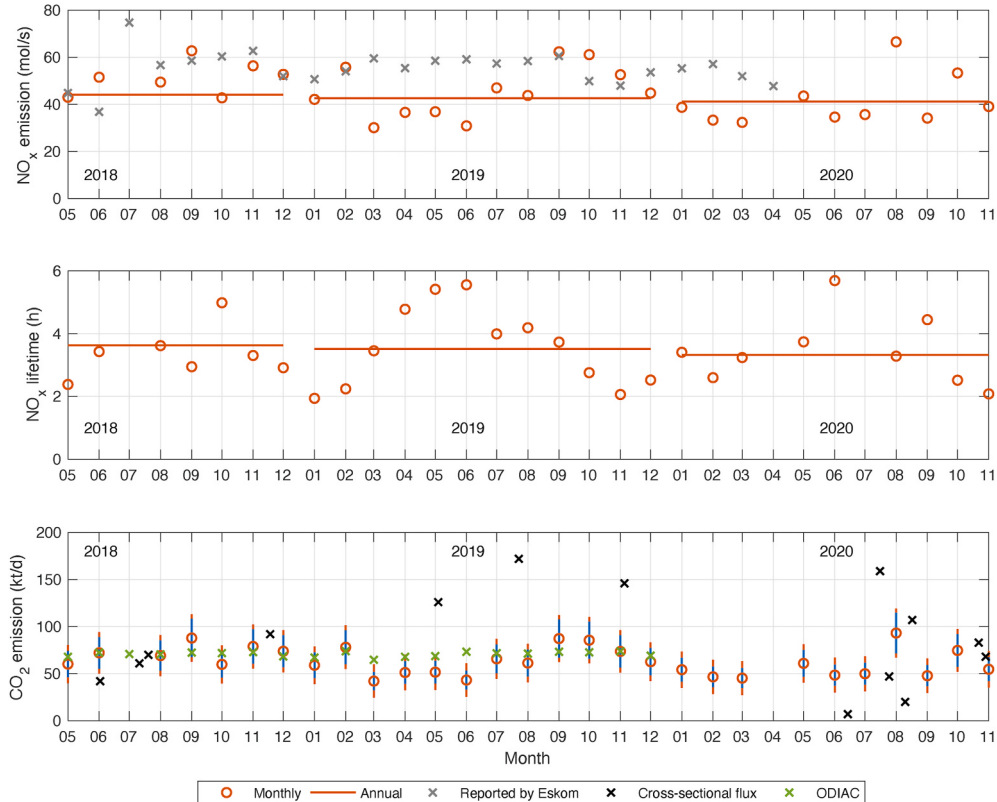


Fig. 6. Top and middle panel: NO_x emission and lifetime estimates, respectively. Bottom panel: CO_2 emission estimates.

CO_2 and NO_2 observed and simulated data. Also, the approach does not need explicit use of wind information. On the contrary, both the cross-sectional flux and Gaussian plume model methods include manual adjustments of the wind direction or directly depend on the wind information. In our approach for the derivation of the emission ratios, the meteorological fields are used implicitly in the Lagrangian model.

The application of the NO_x -to- CO_2 emission ratio to the TROPOMI-based NO_x emission estimate, allowed the estimation of monthly CO_2 emissions, which are consistent with the ODIAC inventory values and their seasonal variability.

The results shown in this paper highlight that quite accurate atmospheric modeling and knowledge of the NO_x lifetime are needed to derive the NO_x -to- CO_2 emission ratios. The approach is also rather general, and could be applied to other point sources or to megacities, although for the latter, a slightly different modeling approach has to be taken (Wu et al., 2020; Shekhar et al., 2020). If the method is applied to larger areas with multiple sources, the obtained value will include a mixed contribution of these sources. For the future, we foresee an increasing amount of collocations available for the application of this method, especially making use of novel observation systems like the OCO-3 Snapshot Area Maps, where several sources can be targeted at high resolution. In addition, wide-swath instruments like the planned Copernicus CO_2 monitoring mission (CO2M) will provide simultaneous NO_2 and CO_2 observations. For the application to these novel observation systems, the method presented here could be also revisited, as multiple cross-sections per collocation would be available.

CRediT authorship contribution statement

Janne Hakkarainen: Conceptualization, Methodology, Software, Formal analysis, Writing – original draft, Writing – review & editing. **Monika E. Szelag:** Methodology, Software, Formal analysis, Writing – review & editing. **Iolanda Ialongo:** Methodology, Formal analysis, Writing – original draft, Writing – review & editing. **Christian Retscher:** Project administration, Writing – review & editing. **Tomo-hiro Oda:** Data curation, Writing – review & editing. **David Crisp:** Data curation, Writing – review & editing.

Declaration of competing interest

The authors declare that they have no known competing financial interests or personal relationships that could have appeared to influence the work reported in this paper.

Acknowledgement

The main part of this study was funded by the European Space Agency via DACES project. We also acknowledge the funding from the Academy of Finland (projects 336798, 337552 and 331829) and the European Union's H2020 projects e-shape (grant no. 820852) and CoCo2 (grant no. 958927). Part of this work was performed at the Jet Propulsion Laboratory, California Institute of Technology, under contract with the National Aeronautics and Space Administration. Government Sponsorship Acknowledged. T. O. is supported by the NASA's Carbon Cycle Science program (grant no. NNX14AM76G) and the Orbiting Carbon Observatory (grant no. 80NSSC18K1313). J. H. thanks Henrik Virta for helping-in with the ERA5 wind data.

Appendix A. Supplementary data

Supplementary data related to this article can be found at <https://doi.org/10.1016/j.aeaoa.2021.100110>.

References

- Beirle, S., Boersma, K.F., Platt, U., Lawrence, M.G., Wagner, T., 2011. Megacity emissions and lifetimes of nitrogen oxides probed from space. *Science* 333, 1737–1739. <https://doi.org/10.1126/science.1207824>.
- Beirle, S., Borger, C., Dörner, S., Li, A., Hu, Z., Liu, F., Wang, Y., Wagner, T., 2019. Pinpointing nitrogen oxide emissions from space. *Science Advances* 5. <https://doi.org/10.1126/sciadv.aax9800>.
- Crisp, D., Pollock, H.R., Rosenberg, R., Chapsky, L., Lee, R.A.M., Oyaafuso, F.A., Frankenberg, C., O'Dell, C.W., Bruegge, C.J., Doran, G.B., Eldering, A., Fisher, B.M., Fu, D., Gunson, M.R., Mandrake, L., Osterman, G.B., Schwandner, F.M., Sun, K., Taylor, T.E., Wennberg, P.O., Wunch, D., 2017. The on-orbit performance of the Orbiting Carbon Observatory-2 (OCO-2) instrument and its radiometrically calibrated products. *Atmospheric Measurement Techniques* 10, 59–81. <https://doi.org/10.5194/amt-10-59-2017>.
- de Foy, B., Wilkins, J.L., Lu, Z., Streets, D.G., Duncan, B.N., 2014. Model evaluation of methods for estimating surface emissions and chemical lifetimes from satellite data. *Atmos. Environ.* 98, 66–77. <https://doi.org/10.1016/j.atmosenv.2014.08.051>.
- Eldering, A., Taylor, T.E., O'Dell, C.W., Pavlick, R., 2019. The OCO-3 mission: measurement objectives and expected performance based on 1 year of simulated data. *Atmospheric Measurement Techniques* 12, 2341–2370. <https://doi.org/10.5194/amt-12-2341-2019>.
- Eldering, A., Wennberg, P.O., Crisp, D., Schimel, D.S., Gunson, M.R., Chatterjee, A., Liu, J., Schwandner, F.M., Sun, Y., O'Dell, C.W., Frankenberg, C., Taylor, T., Fisher, B., Osterman, G.B., Wunch, D., Hakkarainen, J., Tamminen, J., Weir, B., 2017. The Orbiting Carbon Observatory-2 early science investigations of regional carbon dioxide fluxes. *Science* 358. <https://doi.org/10.1126/science.aam5745>.
- Fioletov, V.E., McLinden, C.A., Krotkov, N., Li, C., 2015. Lifetimes and emissions of SO_2 from point sources estimated from OMI. *Geophys. Res. Lett.* 42, 1969–1976. <https://doi.org/10.1002/2015GL063148>.
- Georgoulis, A.K., van der A, R.J., Stammes, P., Boersma, K.F., Eskes, H.J., 2019. Trends and trend reversal detection in 2 decades of tropospheric NO_2 satellite observations. *Atmos. Chem. Phys.* 19, 6269–6294. <https://doi.org/10.5194/acp-19-6269-2019>.
- Goldberg, D.L., Anenberg, S.C., Griffin, D., McLinden, C.A., Lu, Z., Streets, D.G., 2020. Disentangling the impact of the COVID-19 lockdowns on urban NO_2 from natural variability. *Geophys. Res. Lett.* 47, e2020GL089269 <https://doi.org/10.1029/2020GL089269>.
- Goldberg, D.L., Lu, Z., Streets, D.G., de Foy, B., Griffin, D., McLinden, C.A., Lamsal, L.N., Krotkov, N.A., Eskes, H., 2019. Enhanced capabilities of TROPOMI NO_2 : estimating NO_x from north American cities and power plants. *Environ. Sci. Technol.* 53, 12594–12601. <https://doi.org/10.1021/acs.est.9b04488>.
- Hakkarainen, J., Ialongo, I., Maksyutov, S., Crisp, D., 2019. Analysis of four years of global XCO_2 anomalies as seen by orbiting carbon observatory-2. *Rem. Sens.* 11, 850. <https://doi.org/10.3390/rs11070850>.
- Hakkarainen, J., Ialongo, I., Tamminen, J., 2016. Direct space-based observations of anthropogenic CO_2 emission areas from OCO-2. *Geophys. Res. Lett.* 43 (11) <https://doi.org/10.1002/2016GL070885>, 400–11,406.
- Hoesly, R.M., Smith, S.J., Feng, L., Klimont, Z., Janssens-Maenhout, G., Pitkanen, T., Seibert, J.J., Vu, L., Andres, R.J., Bolt, R.M., Bond, T.C., Dawidowski, L., Kholod, N., Kurokawa, J.I., Li, M., Liu, L., Lu, Z., Moura, M.C.P., O'Rourke, P.R., Zhang, Q., 2018. Historical (1750–2014) anthropogenic emissions of reactive gases and aerosols from the Community Emissions Data System (CEDS). *Geosci. Model Dev. (GMD)* 11, 369–408. <https://doi.org/10.5194/gmd-11-369-2018>.
- Hoffmann, L., Günther, G., Li, D., Stein, O., Wu, X., Griessbach, S., Heng, Y., Konopka, P., Müller, R., Vogel, B., Wright, J.S., 2019. From ERA-Interim to ERA5: the considerable impact of ECMWF's next-generation reanalysis on Lagrangian transport simulations. *Atmos. Chem. Phys.* 19, 3097–3124. <https://doi.org/10.5194/acp-19-3097-2019>.
- Johnson, M.S., Schwandner, F.M., Potter, C.S., Nguyen, H.M., Bell, E., Nelson, R.R., Philip, S., O'Dell, C.W., 2020. Carbon dioxide emissions during the 2018 Kilauea volcano eruption estimated using OCO-2 satellite retrievals. *Geophysical Research Letters* n/a, e2020GL090507. <https://doi.org/10.1029/2020GL090507>.
- Kiel, M., Eldering, A., Roten, D.D., Lin, J.C., Feng, S., Lei, R., Lauvaux, T., Oda, T., Roehl, C.M., Blavier, J.F., Iraci, L.T., 2021. Urban-focused satellite CO_2 observations from the orbiting carbon observatory-3: a first look at the los angeles megacity. *Rem. Sens. Environ.* 258, 112314 <https://doi.org/10.1016/j.rse.2021.112314>.
- Kiel, M., O'Dell, C.W., Fisher, B., Eldering, A., Nassar, R., MacDonald, C.G., Wennberg, P.O., 2019. How bias correction goes wrong: measurement of XCO_2 affected by erroneous surface pressure estimates. *Atmospheric Measurement Techniques* 12, 2241–2259. <https://doi.org/10.5194/amt-12-2241-2019>.
- Krotkov, N.A., McLinden, C.A., Li, C., Lamsal, L.N., Celarier, E.A., Marchenko, S.V., Swartz, W.H., Bucsela, E.J., Joiner, J., Duncan, B.N., Boersma, K.F., Vreekind, J.P., Levelt, P.F., Fioletov, V.E., Dickerson, R.R., He, H., Lu, Z., Streets, D.G., 2016. Aura OMI observations of regional SO_2 and NO_2 pollution changes from 2005 to 2015. *Atmos. Chem. Phys.* 16, 4605–4629. <https://doi.org/10.5194/acp-16-4605-2016>.
- Liu, F., Duncan, B.N., Krotkov, N.A., Lamsal, L.N., Beirle, S., Griffin, D., McLinden, C.A., Goldberg, D.L., Lu, Z., 2020. A methodology to constrain carbon dioxide emissions from coal-fired power plants using satellite observations of co-emitted nitrogen dioxide. *Atmos. Chem. Phys.* 20, 99–116. <https://doi.org/10.5194/acp-20-99-2020>.
- Lorente, A., Boersma, K.F., Eskes, H.J., Vreekind, J.P., van Geffen, J.H.G.M., de Zeeuw, M.B., Denier van der Gon, H.A.C., Beirle, S., Krol, M.C., 2019. Quantification of nitrogen oxides emissions from build-up of pollution over Paris with TROPOMI. *Sci. Rep.* 9, 20033. <https://doi.org/10.1038/s41598-019-56428-5>.
- Nassar, R., Hill, T.G., McLinden, C.A., Wunch, D., Jones, D.B.A., Crisp, D., 2017. Quantifying CO_2 emissions from individual power plants from space. *Geophys. Res. Lett.* 44 (10) <https://doi.org/10.1002/2017GL074702>, 045–10,053.

- Oda, T., Maksyutov, S., Andres, R.J., 2018. The Open-source Data Inventory for Anthropogenic CO₂, version 2016 (ODIAC2016): a global monthly fossil fuel CO₂ gridded emissions data product for tracer transport simulations and surface flux inversions. *Earth Syst. Sci. Data* 10, 87–107. <https://doi.org/10.5194/essd-10-87-2018>.
- O'Dell, C.W., Eldering, A., Wennberg, P.O., Crisp, D., Gunson, M.R., Fisher, B., Frankenberg, C., Kiel, M., Lindqvist, H., Mandrake, L., Merrelli, A., Natraj, V., Nelson, R.R., Osterman, G.B., Payne, V.H., Taylor, T.E., Wunch, D., Drouin, B.J., Oyafuso, F., Chang, A., McDuffie, J., Smyth, M., Baker, D.F., Basu, S., Chevallier, F., Crowell, S.M.R., Feng, L., Palmer, P.I., Dubey, M., García, O.E., Griffith, D.W.T., Hase, F., Iraci, L.T., Kivi, R., Morino, I., Notholt, J., Ohyama, H., Petri, C., Roehl, C. M., Sha, M.K., Strong, K., Sussmann, R., Te, Y., Uchino, O., Velazco, V.A., 2018. Improved retrievals of carbon dioxide from Orbiting Carbon Observatory-2 with the version 8 ACOS algorithm. *Atmospheric Measurement Techniques* 11, 6539–6576. <https://doi.org/10.5194/amt-11-6539-2018>.
- Park, H., Jeong, S., Park, H., Labzovskii, L.D., Bowman, K.W., 2021. An assessment of emission characteristics of Northern Hemisphere cities using spaceborne observations of CO₂, CO, and NO₂. *Rem. Sens. Environ.* 254, 112246. <https://doi.org/10.1016/j.rse.2020.112246>.
- Pisso, I., Sollum, E., Grythe, H., Kristiansen, N.I., Cassiani, M., Eckhardt, S., Arnold, D., Morton, D., Thompson, R.L., Groot Zwaaftink, C.D., Evangelou, N., Sodemann, H., Haimberger, L., Henne, S., Brunner, D., Burkhardt, J.F., Fouilloux, A., Brioude, J., Philipp, A., Seibert, P., Stohl, A., 2019. The Lagrangian particle dispersion model FLEXPART version 10.4. *Geosci. Model Dev. (GMD)* 12, 4955–4997. <https://doi.org/10.5194/gmd-12-4955-2019>.
- Reuter, M., Buchwitz, M., Hilboll, A., Richter, A., Schneising, O., Hilker, M., Heymann, J., Bovensmann, H., Burrows, J.P., 2014. Decreasing emissions of NO_x relative to CO₂ in East Asia inferred from satellite observations. *Nat. Geosci.* 7, 792–795. <https://doi.org/10.1038/ngeo2257>.
- Reuter, M., Buchwitz, M., Schneising, O., Krautwurst, S., O'Dell, C.W., Richter, A., Bovensmann, H., Burrows, J.P., 2019. Towards monitoring localized CO₂ emissions from space: co-located regional CO₂ and NO₂ enhancements observed by the OCO-2 and SSP satellites. *Atmos. Chem. Phys.* 19, 9371–9383. <https://doi.org/10.5194/acp-19-9371-2019>.
- Shekhar, A., Chen, J., Paetzold, J.C., Dietrich, F., Zhao, X., Bhattacharjee, S., Ruisinger, V., Wofsy, S.C., 2020. Anthropogenic CO₂ emissions assessment of Nile Delta using XCO₂ and SIF data from OCO-2 satellite. *Environ. Res. Lett.* 15, 095010. <https://doi.org/10.1088/0268-1133/abf9cf>. URL:
- Stohl, A., Forster, C., Frank, A., Seibert, P., Wotawa, G., 2005. Technical note: the Lagrangian particle dispersion model FLEXPART version 6.2. *Atmos. Chem. Phys.* 5, 2461–2474. <https://doi.org/10.5194/acp-5-2461-2005>.
- Streets, D.G., Carty, T., Carmichael, G.R., de Foy, B., Dickerson, R.R., Duncan, B.N., Edwards, D.P., Haynes, J.A., Henze, D.K., Houyoux, M.R., Jacob, D.J., Krotkov, N.A., Lamsal, L.N., Liu, Y., Lu, Z., Martin, R.V., Pfister, G.G., Pinder, R.W., Salawitch, R.J., Wecht, K.J., 2013. Emissions estimation from satellite retrievals: a review of current capability. *Atmos. Environ.* 77, 1011–1042. <https://doi.org/10.1016/j.atmosenv.2013.05.051>.
- Tong, D., Zhang, Q., Davis, S.J., Liu, F., Zheng, B., Geng, G., Xue, T., Li, M., Hong, C., Lu, Z., Streets, D.G., Guan, D., He, K., 2018. Targeted emission reductions from global super-polluting power plant units. *Nature Sustainability* 1, 59–68. <https://doi.org/10.1038/s41893-017-0003-y>.
- van Geffen, J.H.G.M., Eskes, H.J., Boersma, K.F., Maasakkers, J.D., Veefkind, J.P., 2019. TROPOMI ATBD of the total and tropospheric NO₂ data products. Technical Report. URL: <https://sentinel.esa.int/documents/247904/2476257/Sentinel-5P-TROPOMI-ATBD-NO2-data-products>.
- Varon, D.J., Jacob, D.J., McKeever, J., Jervis, D., Durak, B.O.A., Xia, Y., Huang, Y., 2018. Quantifying methane point sources from fine-scale satellite observations of atmospheric methane plumes. *Atmospheric Measurement Techniques* 11, 5673–5686. <https://doi.org/10.5194/amt-11-5673-2018>.
- Veefkind, J., Aben, I., McMullan, K., Förster, H., de Vries, J., Otter, G., Claas, J., Eskes, H., de Haan, J., Kleipool, Q., van Weele, M., Hasekamp, O., Hoogeveen, R., Landgraf, J., Snel, R., Tol, P., Ingmann, P., Voors, R., Kruizinga, B., Vink, R., Visser, H., Levelt, P., 2012. TROPOMI on the ESA Sentinel-5 Precursor: a GMES mission for global observations of the atmospheric composition for climate, air quality and ozone layer applications. *Rem. Sens. Environ.* 120, 70–83. <https://doi.org/10.1016/j.rse.2011.09.027>. the Sentinel Missions - New Opportunities for Science.
- Wu, D., Lin, J.C., Oda, T., Kort, E.A., 2020. Space-based quantification of per capita CO₂ emissions from cities. *Environ. Res. Lett.* 15, 035004. <https://doi.org/10.1088/1748-9326/ab68eb>.
- Wunch, D., Wennberg, P.O., Osterman, G., Fisher, B., Naylor, B., Roehl, C.M., O'Dell, C., Mandrake, L., Viatte, C., Kiel, M., Griffith, D.W.T., Deutscher, N.M., Velazco, V.A., Notholt, J., Warneke, T., Petri, C., De Maziere, M., Sha, M.K., Sussmann, R., Rettinger, M., Pollard, D., Robinson, J., Morino, I., Uchino, O., Hase, F., Blumenstock, T., Feist, D.G., Arnold, S.G., Strong, K., Mendonca, J., Kivi, R., Heikkinen, P., Iraci, L., Podolske, J., Hillyard, P.W., Kawakami, S., Dubey, M.K., Parker, H.A., Sepulveda, E., García, O.E., Te, Y., Jeseck, P., Gunson, M.R., Crisp, D., Eldering, A., 2017. Comparisons of the orbiting carbon observatory-2 (OCO-2) XCO₂ measurements with TCCON. *Atmospheric Measurement Techniques* 10, 2209–2238. <https://doi.org/10.5194/amt-10-2209-2017>.
- Yokota, T., Yoshida, Y., Eguchi, N., Ota, Y., Tanaka, T., Watanabe, H., Maksyutov, S., 2009. Global concentrations of CO₂ and CH₄ retrieved from GOSAT: first preliminary results. *SOLA* 5, 160–163. <https://doi.org/10.2151/sola.2009-041>.
- Zheng, T., Nassar, R., Baxter, M., 2019. Estimating power plant CO₂ emission using OCO-2 XCO₂ and high resolution WRF-Chem simulations. *Environ. Res. Lett.* 14, 085001. <https://doi.org/10.1088/1748-9326/ab25ae>.